Supporting Information

For

Anion dependent thermo-responsive supramolecular superstructures of Cu(II)-macrocycles

Sourenjit Naskar, Barun Jana, Pradyut Ghosh[a]*

[a] *Department of Inorganic Chemistry, Indian Association for the Cultivation of Science*

Table of Contents

1. Materials and methods:

All reagents were used as received from the commercial sources without purification unless otherwise noted. HRMS analysis was performed on a QToF−Micro YA 263 mass spectrometer where ESI (+ve) mode was used. ^{1}H and ^{13}C experiments were carried out on FT-NMR Bruker DPX 300/400MHz NMR spectrometer. ^{1}H-NMR titration experiments were carried out on a 300 MHz Bruker DPX NMR spectrometer. Chemical shifts for ^{1}H and ^{13}CNMR were reported in parts per million (ppm), calibrated to the residual solvent peak set. Absorption spectra were recorded in Perkin Elmer Lambda 950 UV/vis/NIR spectrometer (with a quartz cuvette of path length 1 cm). Scanning electron microscope (SEM) studies were performed through a FESEM instrument (JEOL, JSM 6700F) operating at 5 KV. AFM studies were performed via non-contact mode (Veeco model dicp2) at 300 KHz frequency, by use of 0.01-0.025 ohm.cm antimony doped silicon cantilever (length = 125 μM, width = 35 μM and thickness = 3.75 μM). For microscopic study, samples were prepared by solvent evaporation method. When immediate solvent evaporation was needed then the samples were subjected to vacuum due to relatively higher boiling point of DMF.

Characterization of L:

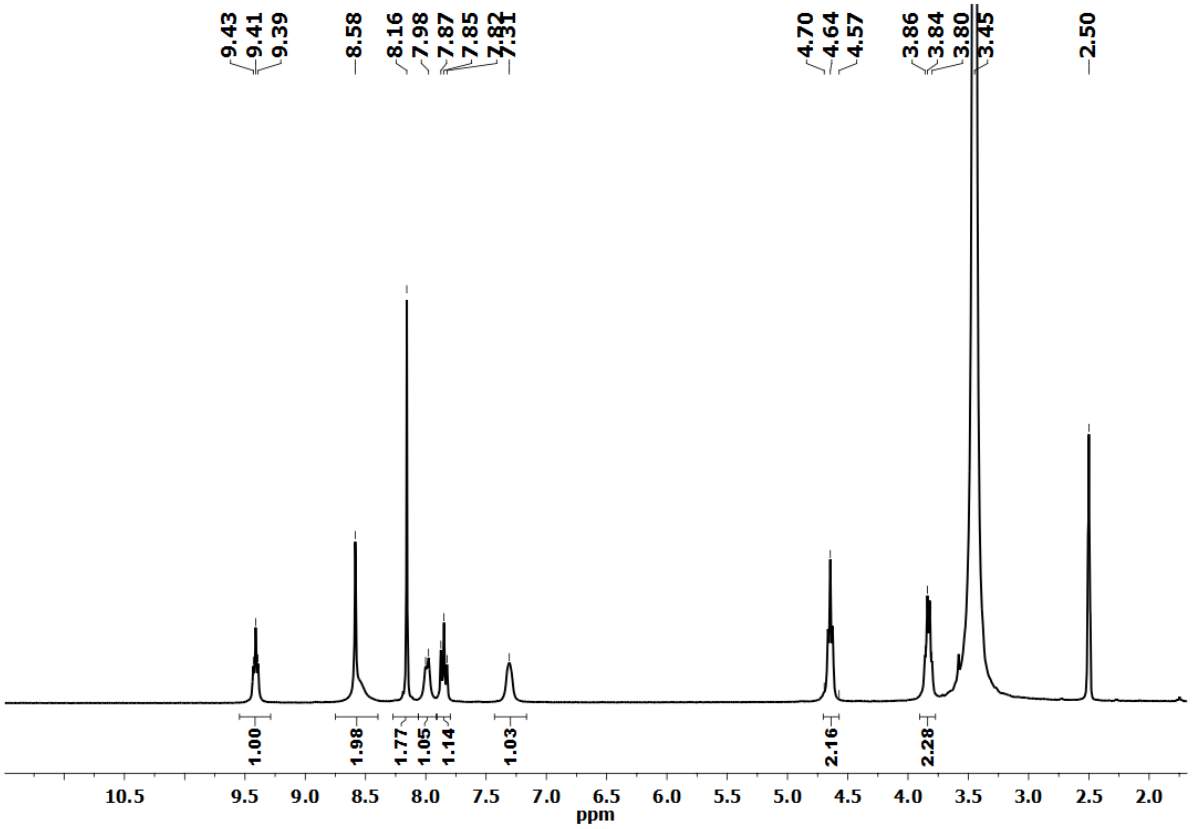

Fig. S1: ^{1}H NMR of **L** in DMSO-d_6.

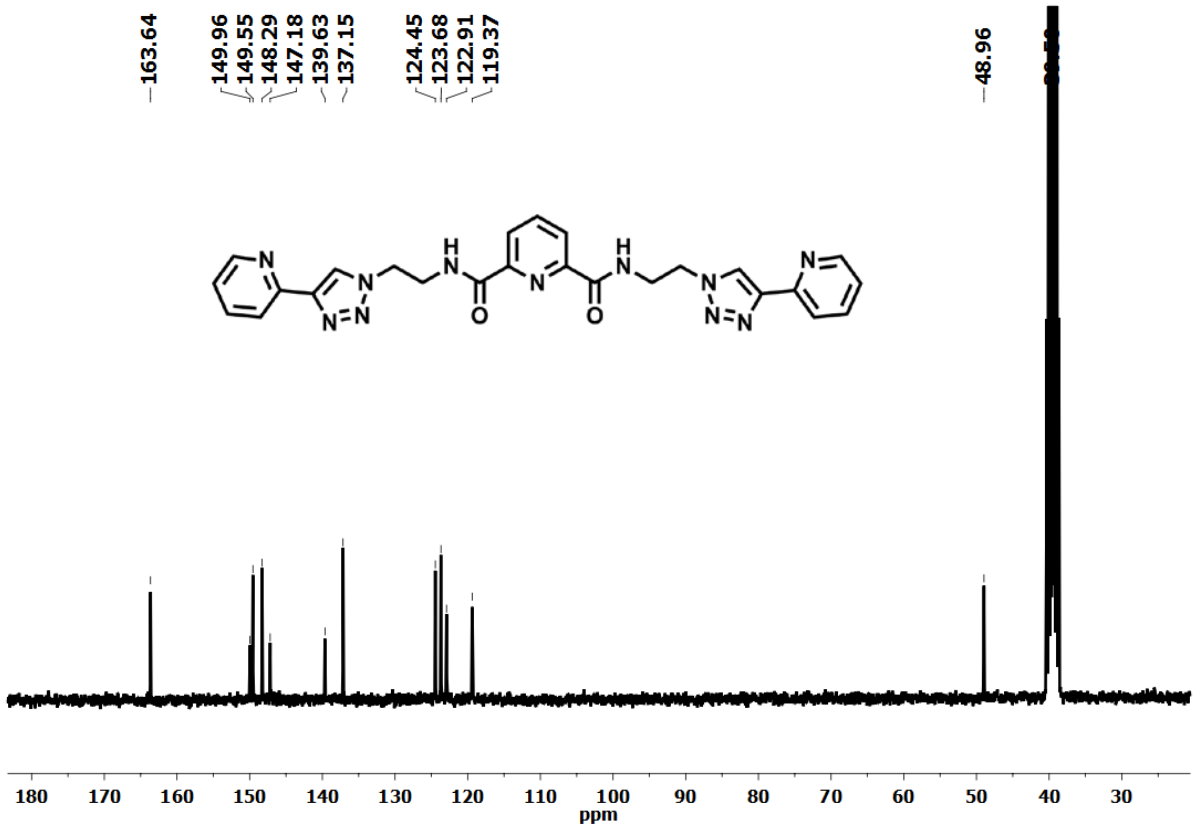

Fig. S2: ^{13}C-NMR of **L** in DMSO-d_6.

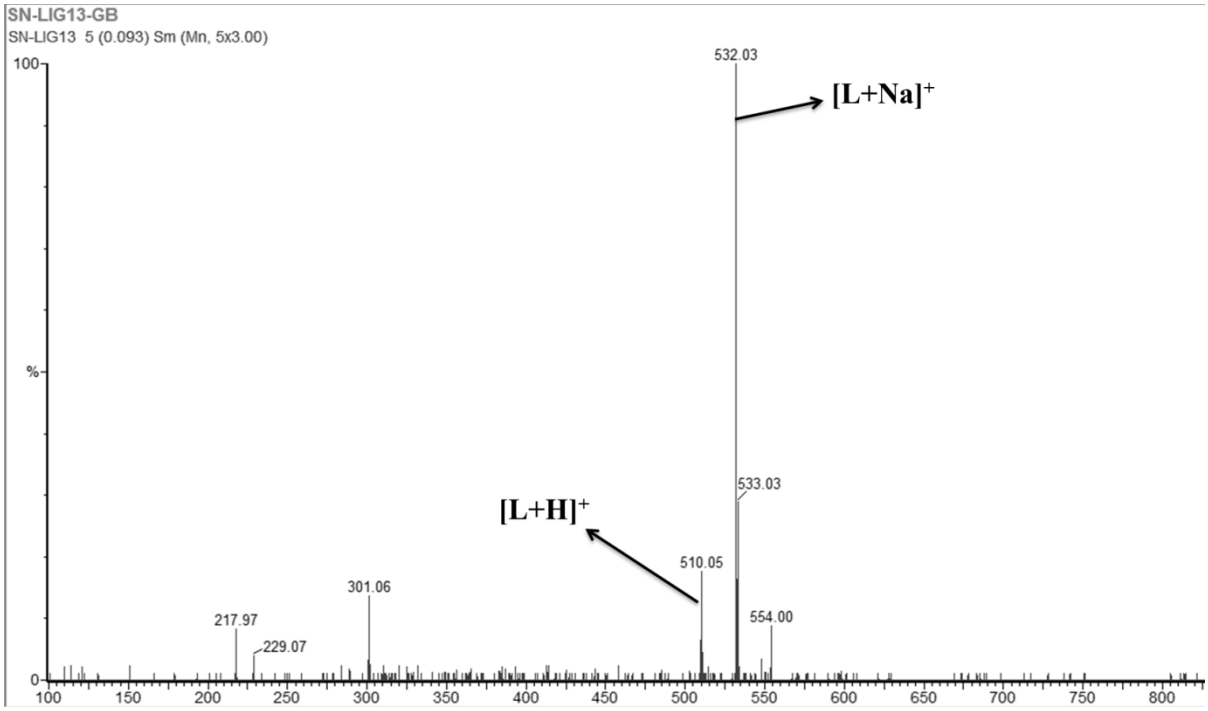

Fig. S3: ESI-MS (+ve) of **L**.

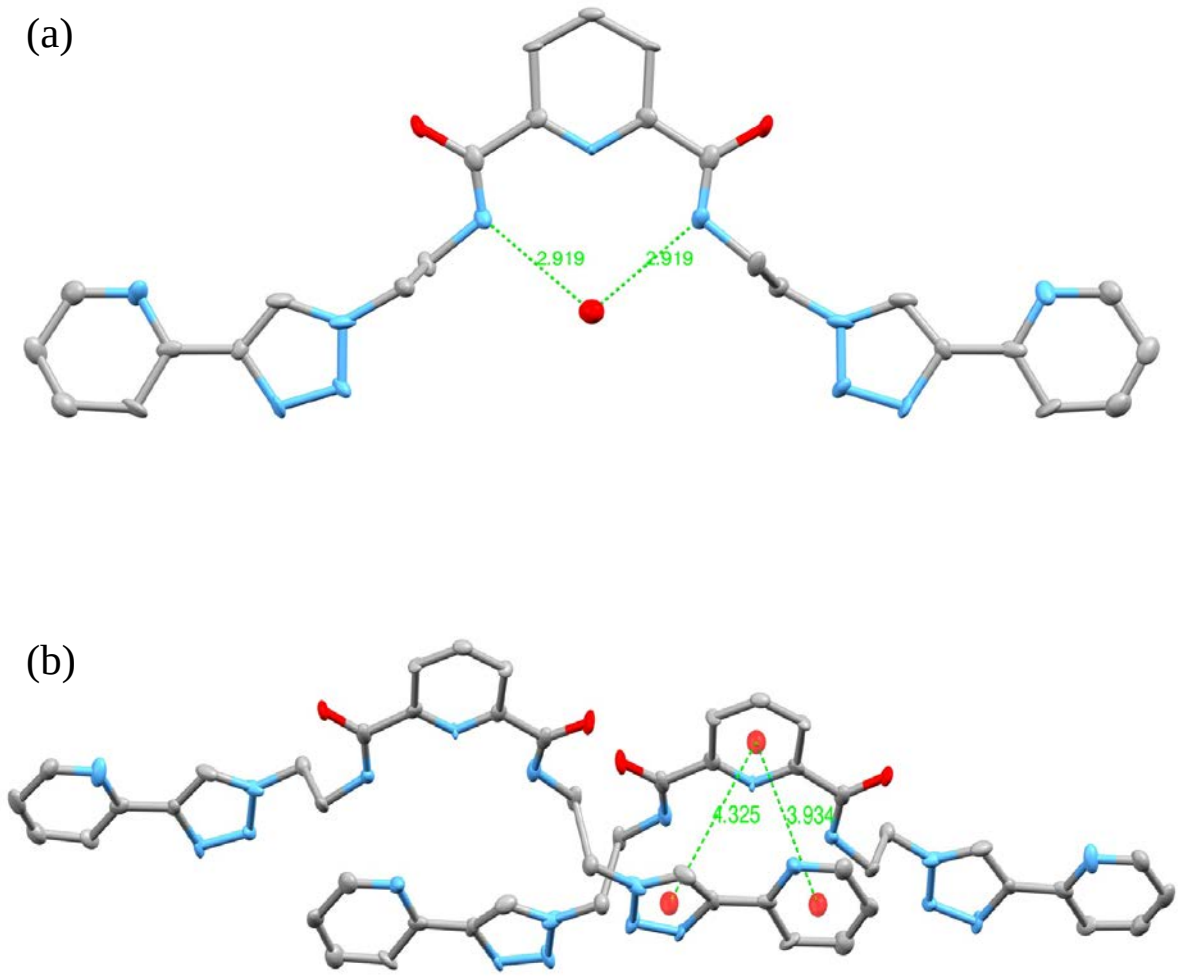

Fig. S4: (a) Molecular structure of **L**, where two amide -CONH units of L very strongly and simultaneously H-bonded (average H-bonding distance $d_{N\text{-}O}$ = 2.91 Å) with a single water molecule in intramolecular manner, further (b) inter-ligand π-π stacking interaction is observed in solid state.

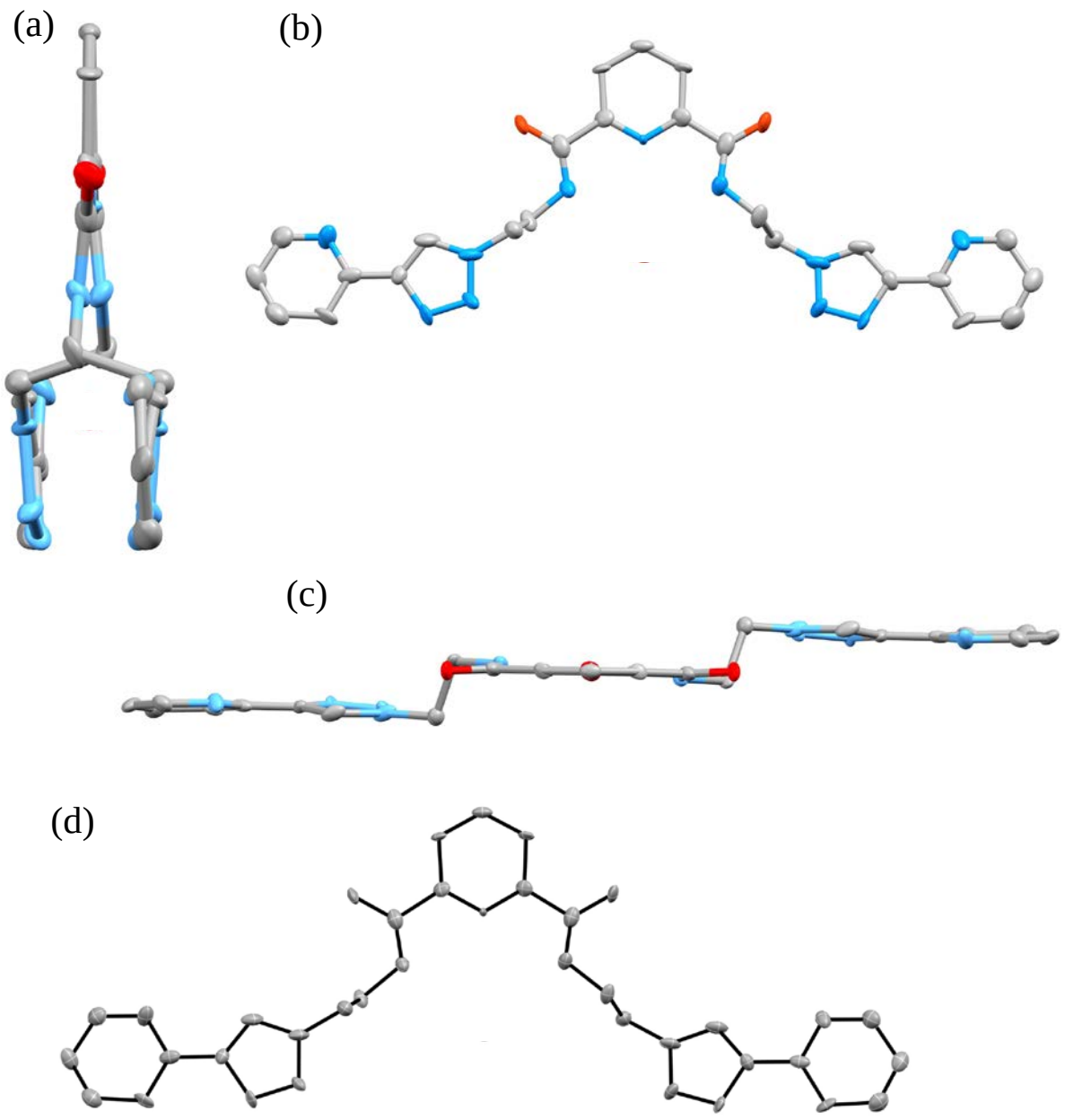

Fig. S5: (a,b,c) Molecular structure of **L** from different axes**,** (d) ORTEP representation of free-ligand **L** (where displacement ellipsoids are drawn at 50% probability level).

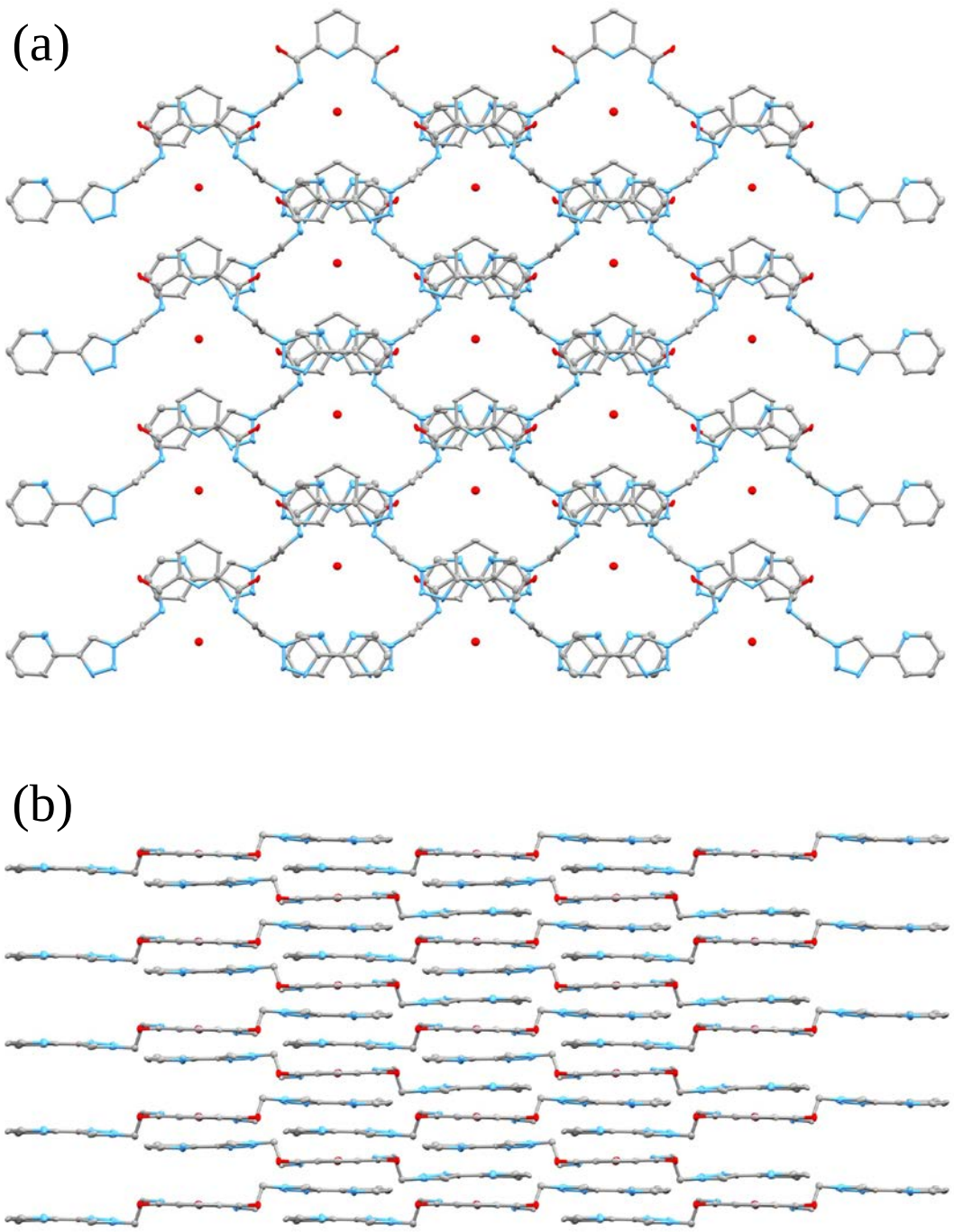

Fig. S6: Packing of the free ligand strands within in solid state of **L**.

L possesses a 2,6-pyridinedicarboxamide unit in the central position to which two terminal pyridyltriazole units are connected via double methylene (-CH_2-) spacer. Presence of such amide and π-π stacking interaction between electron deficient aromatic units generally exhibit interesting morphology. Thus, the field emission scanning electron microscopic (FESEM) study performed with ~7.4×10^{-3} M solution of **L** in DMF. It is found that **L** forms only solid crystalline particles with ~0.5 μm of diameter, though variation of particle sizes is observed.

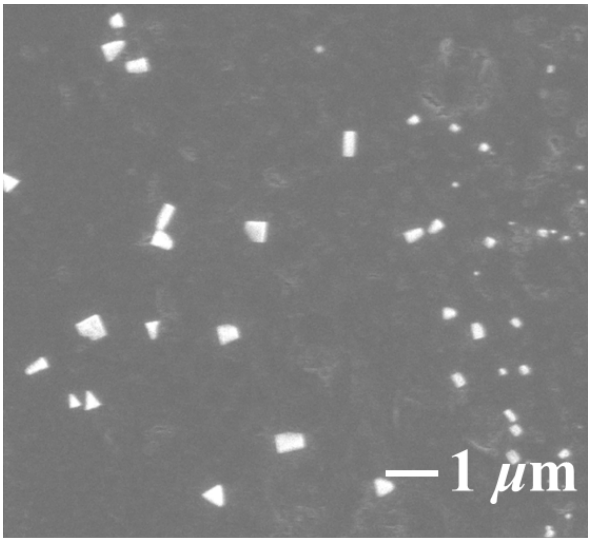

Fig. S7: FESEM study performed with the sample prepared by evaporation of DMF solution of **L**, which shows formation of micro-crystals.

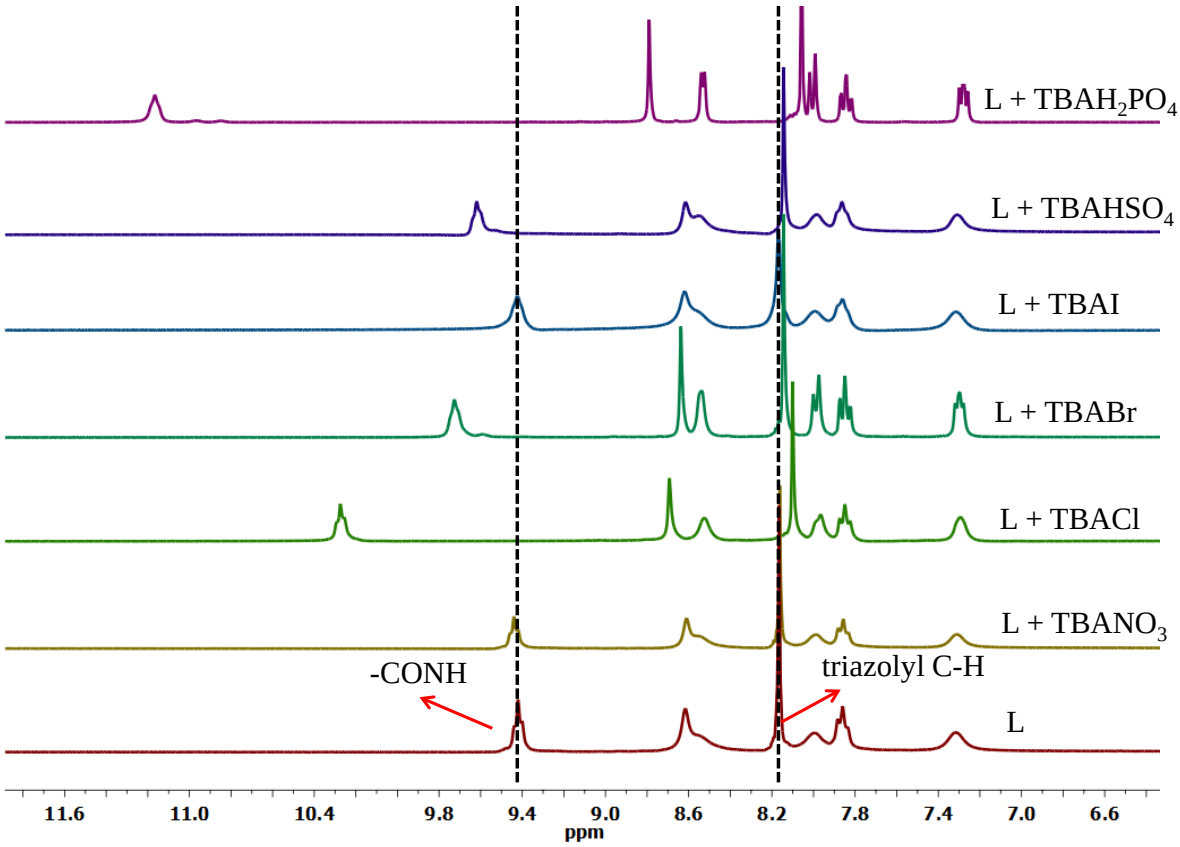

Fig. S8: Qualitative ^{1}H-NMR study with a measured quantity of **L** (~4 mg in 430 μL DMSO-d_6) is treated with a variety of anions with different basicities, having non-interacting tetrabutylammonium counter cation. Interestingly, in presence of excess (~10 equiv) of anions almost no observable shift occurs for the sharp singlet peak at ~8.1 ppm, which corresponding to triazolyl C-H proton (Fig xxx). However, the peak at ~9.4 ppm corresponding to amide –CONH proton is shifted in different extent with different counter anions. For example, the peak shifted to ~9.6, ~9.7, ~10.2 and ~11.1 ppm upon individual treatment of $TBAHSO_4$, TBABr, TBACl, $TBAH_2PO_4$ respectively. Further, no observable shift observed upon treatment of less basic anions such as $TBANO_3$, TBAI and $TBAClO_4$.

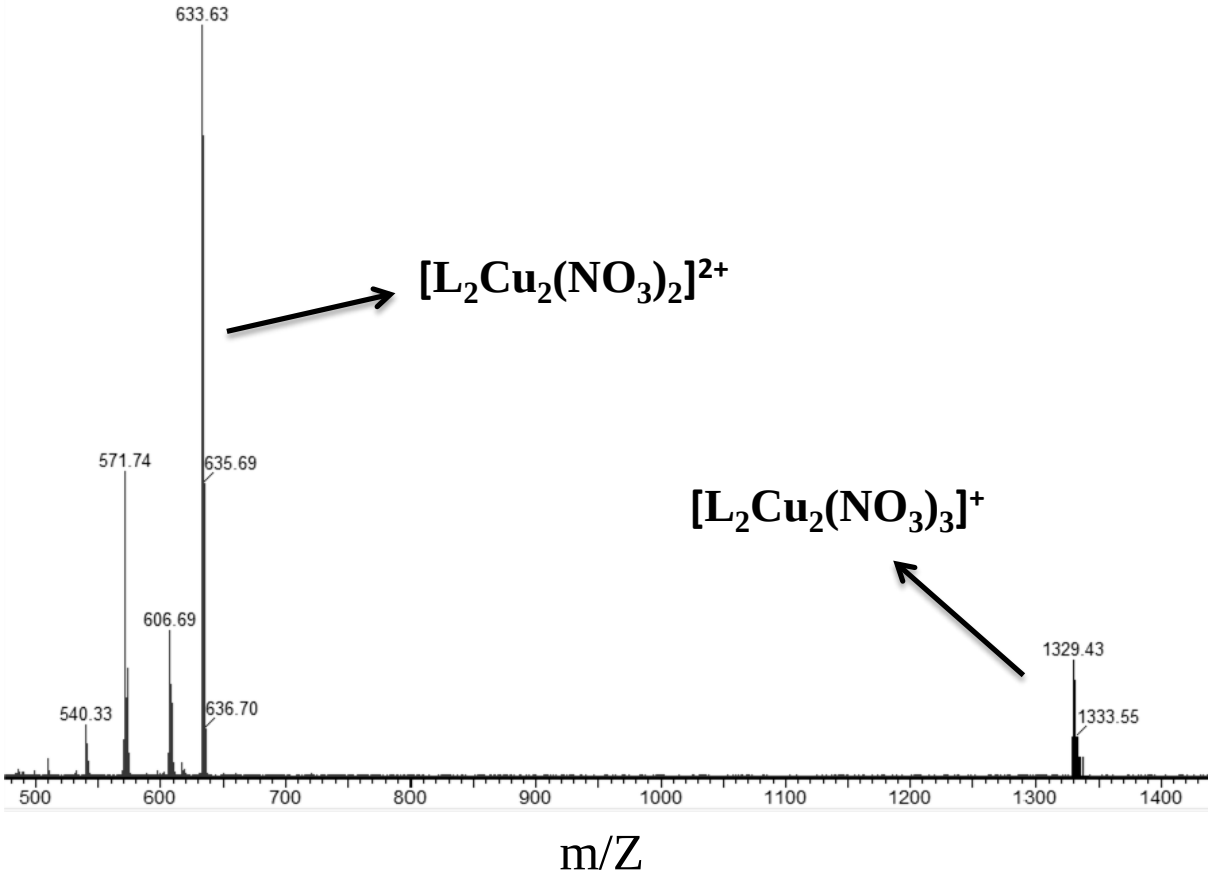

Fig. S9: ESI-MS (+ve) study performed with $[\mathbf{L}_2Cu_2](NO_3)_4$ complex.

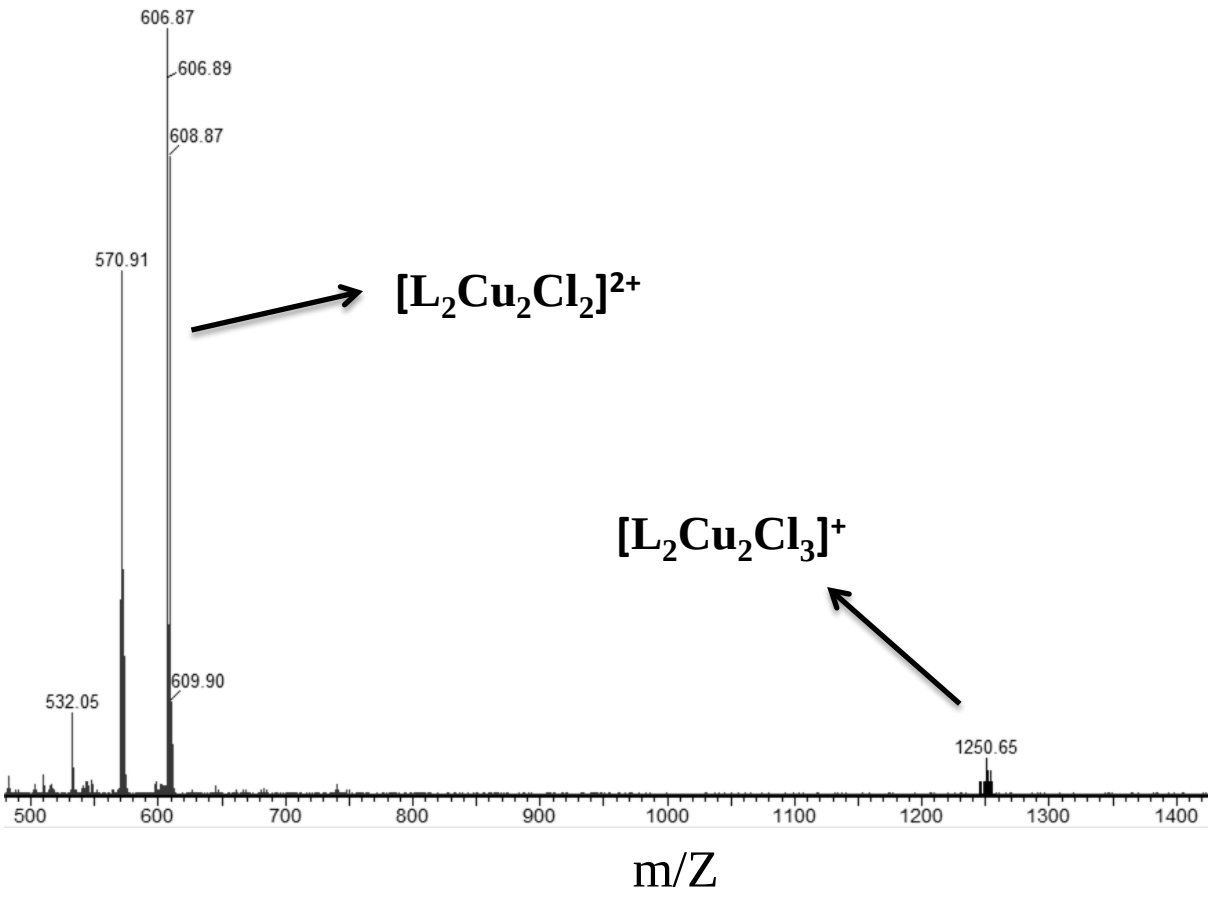

Fig. S10: ESI-MS (+ve) study performed with $[\mathbf{L}_2Cu_2](Cl)_4$ complex.

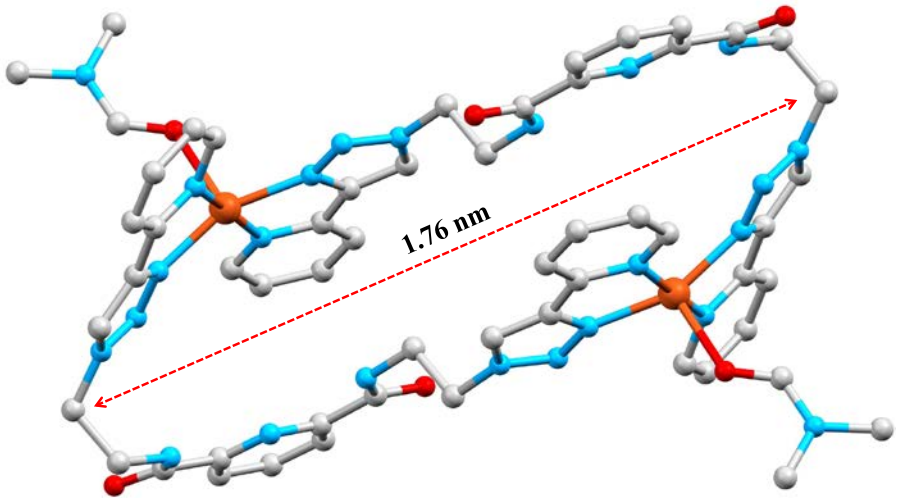

Fig. S11: Dinuclear Cu(II)-macrocycle of $[\mathbf{L}_2Cu_2](ClO_4)_4$ (counter anions and solvent molecules are removed for clarity).

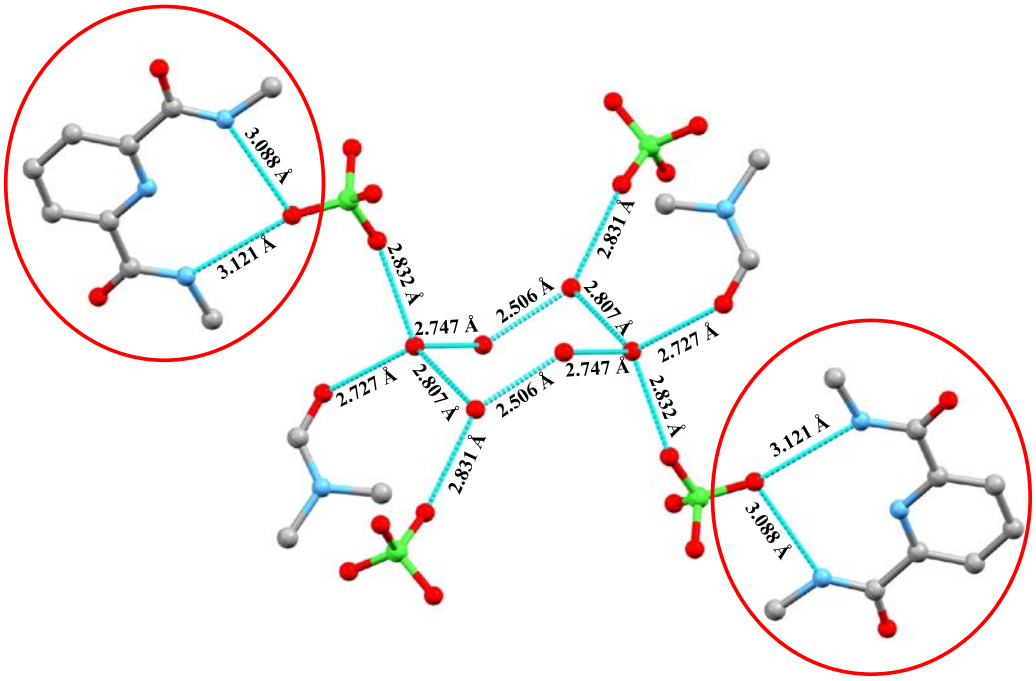

Fig. S12: Formation of 6-membered chair like water cluster, which creates a bridge between two discrete macrocycle of $[\mathbf{L}_2Cu_2](ClO_4)_4$ via anion-coordination.

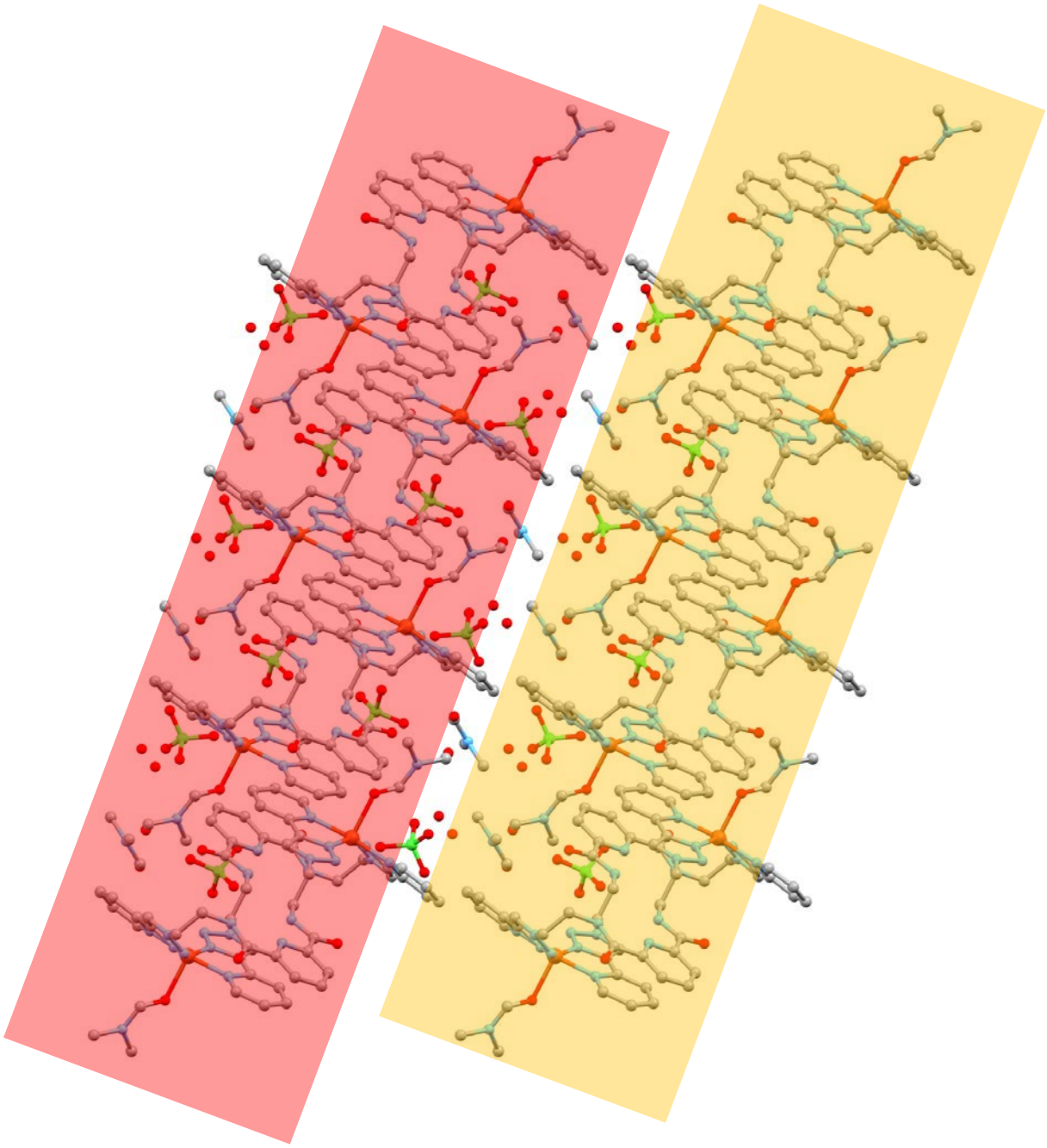

Fig. S13: Packing of $[\mathbf{L}_2Cu_2](ClO_4)_4$ shows the formation of linear chain.

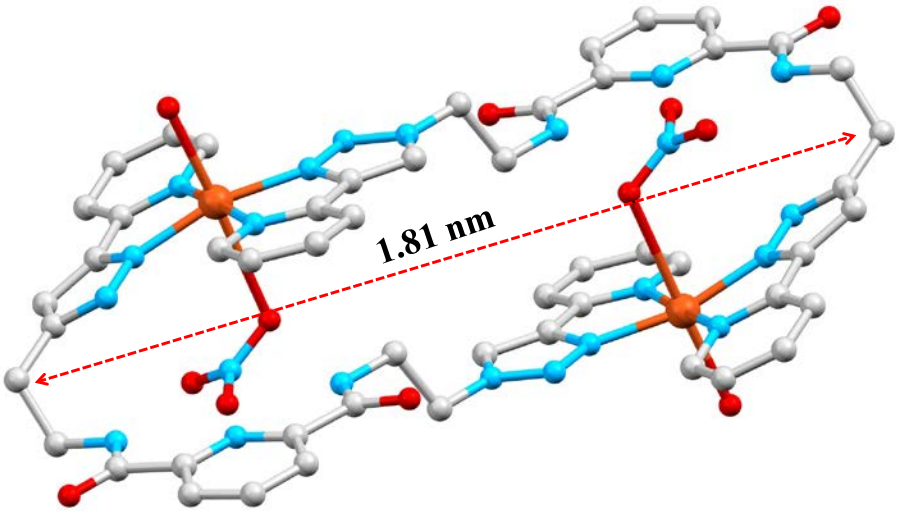

Fig. S14: Dinuclear Cu(II)-macrocycle of $[\mathbf{L}_2Cu_2(NO_3)_2](NO_3)_2$ (counter anions and solvent molecules are removed for clarity).

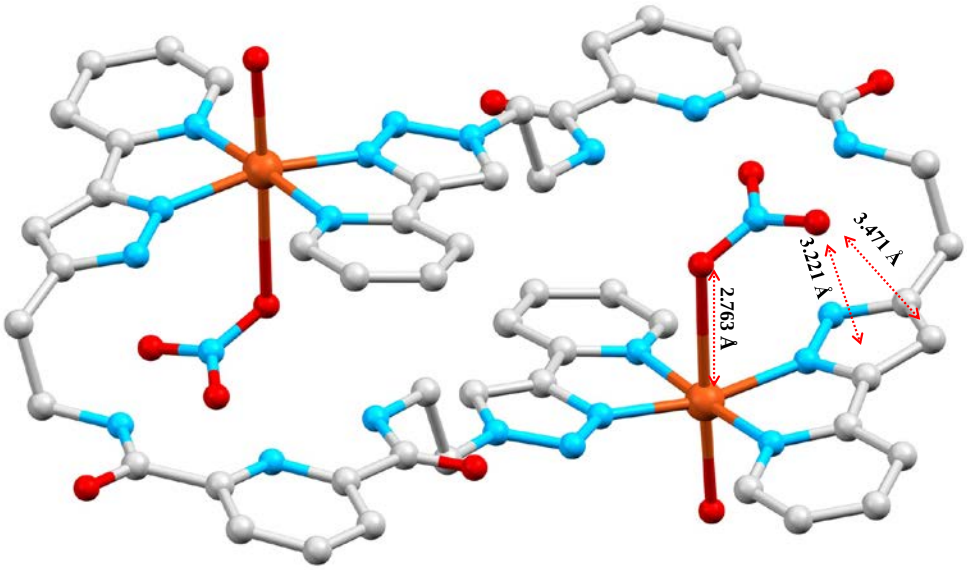

Fig. S15: Weak interaction between the NO_3^- and the Cu(II) center is observed, this metal-coordinated anion also form very strong H-bonding interactions with two –CONH groups of central unit. Additionally, anion-π interaction between NO_3^- and the triazolyl group from metal-coordinated pyridyl-triazole unit.

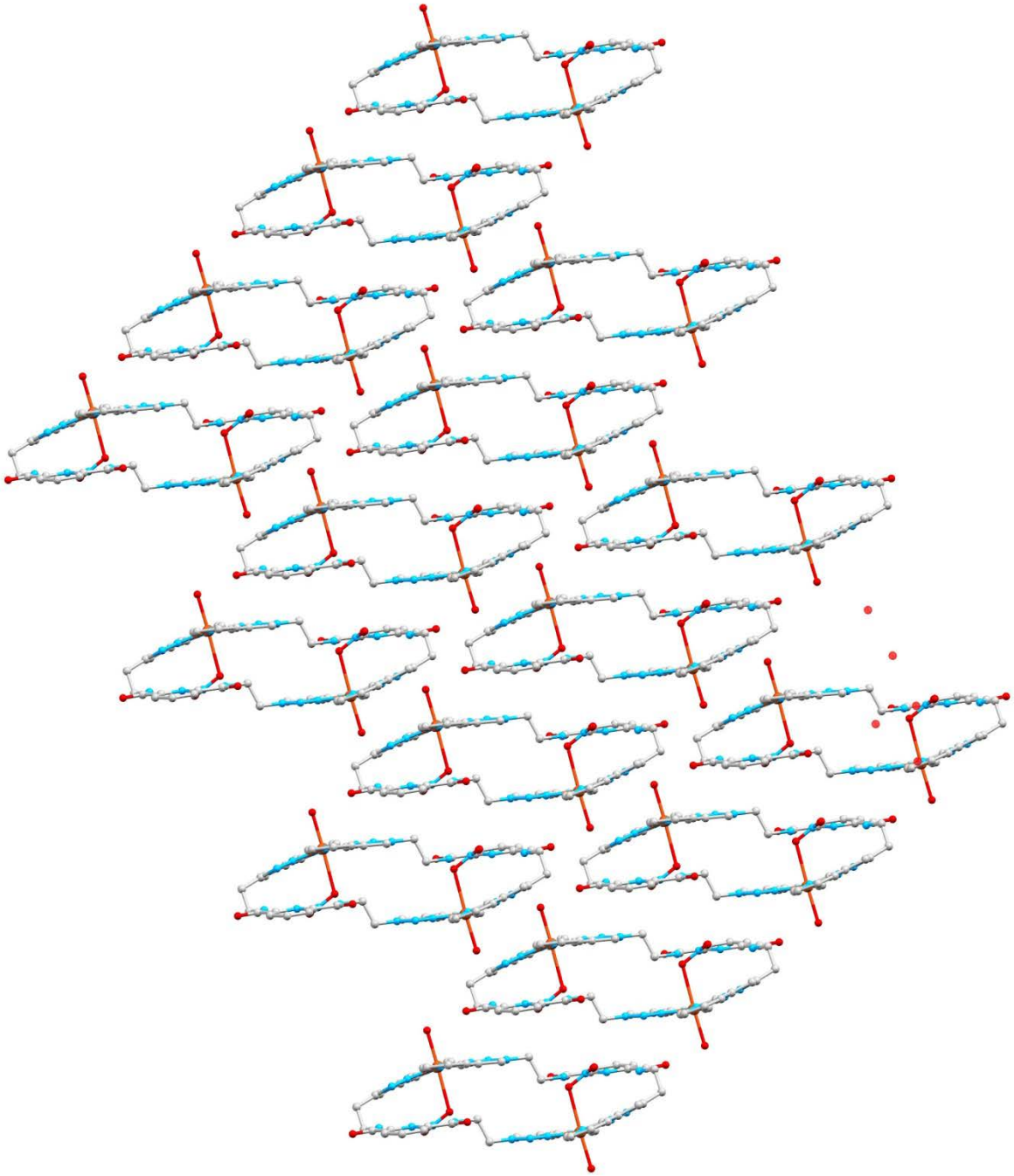

Fig. S16: Packing of discrete macrocycles of $[\mathbf{L}_2Cu_2(NO_3)_2](NO_3)_2$ in the solid state.

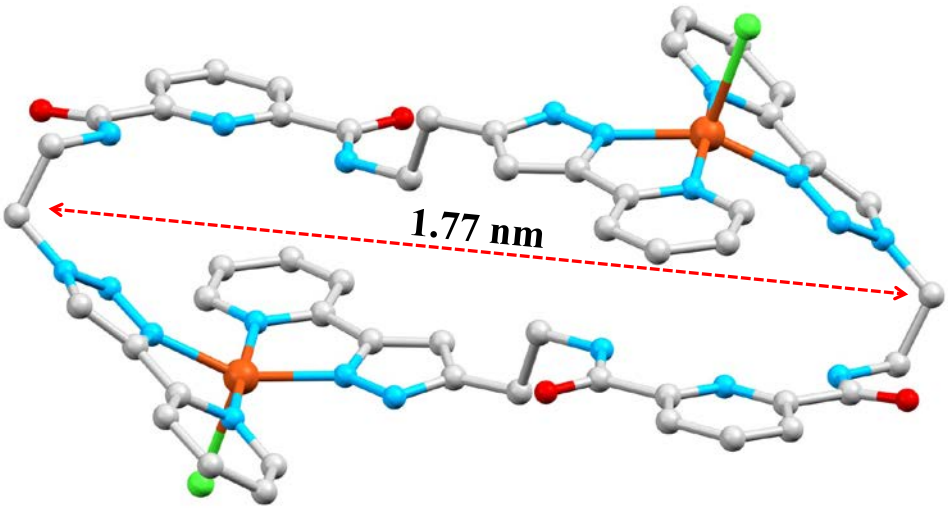

Fig. S17: Dinuclear Cu(II)-macrocycle of $[\mathbf{L}_2Cu_2(Cl)_2](Cl)_2$ (some counter anions and solvent molecules are removed for clarity).

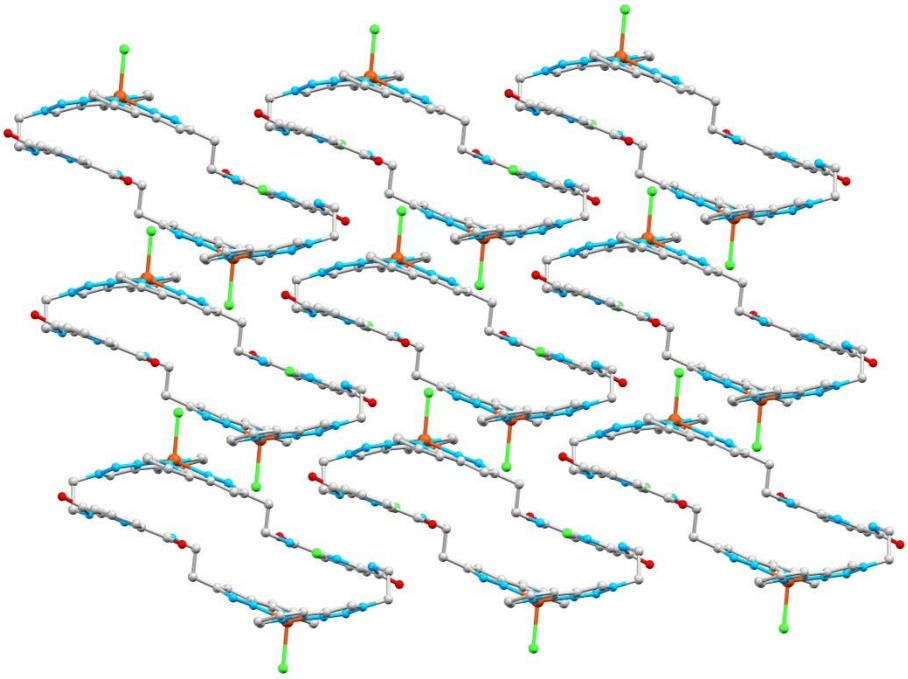

Fig. S18: Packing of discrete macrocycles of $[\mathbf{L}_2Cu_2(Cl)_2](Cl)_2$ in the solid state.

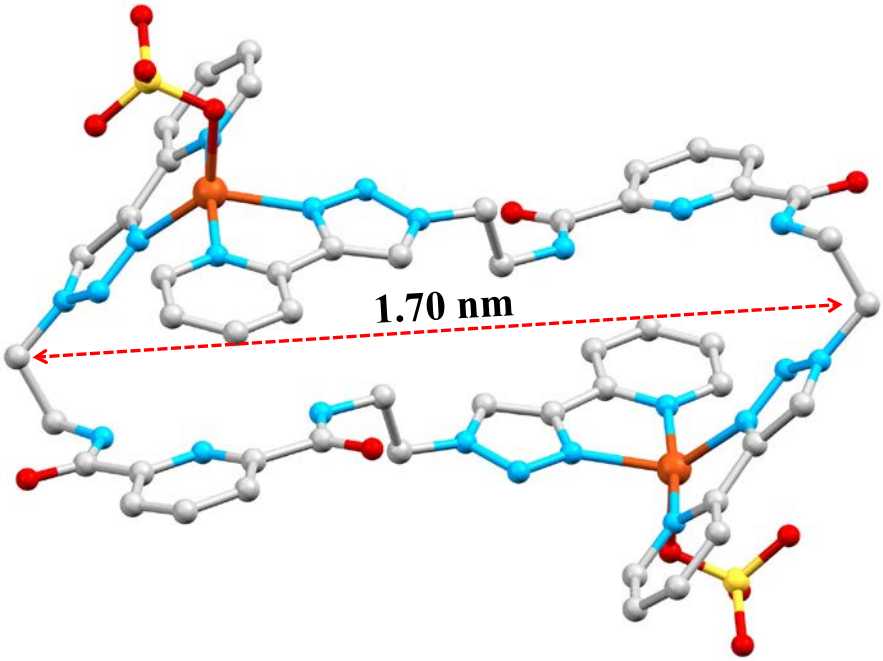

Fig. S19: Dinuclear Cu(II)-macrocycle of [$\mathbf{L}_2Cu_2(SO_4)_2$] (some counter anions and solvent molecules are removed for clarity).

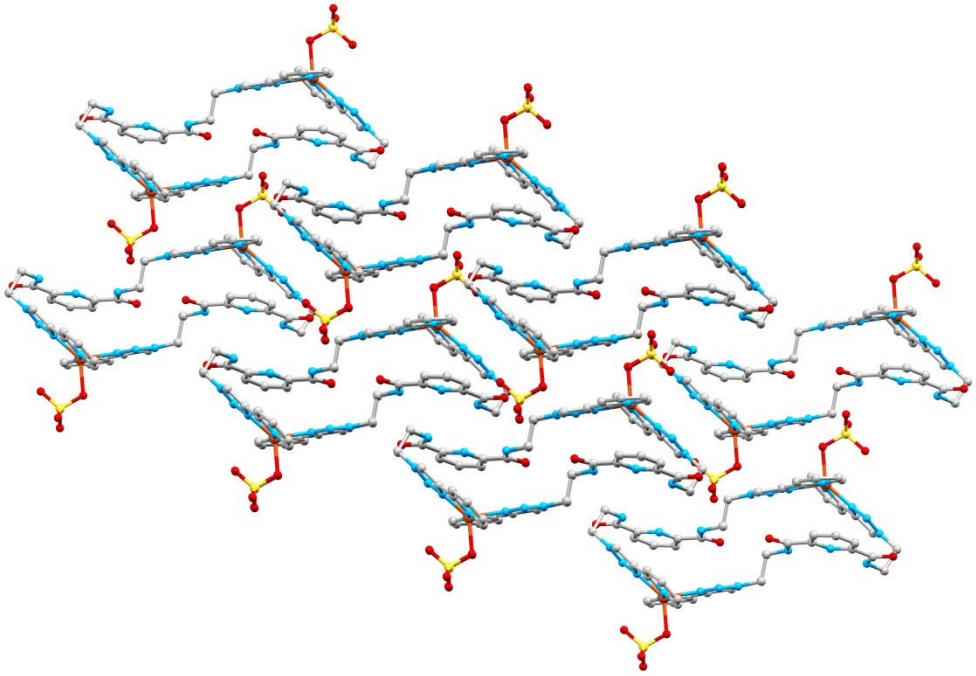

Fig. S20: Packing of discrete macrocycles of [$\mathbf{L}_2Cu_2(SO_4)_2$] in the solid state.

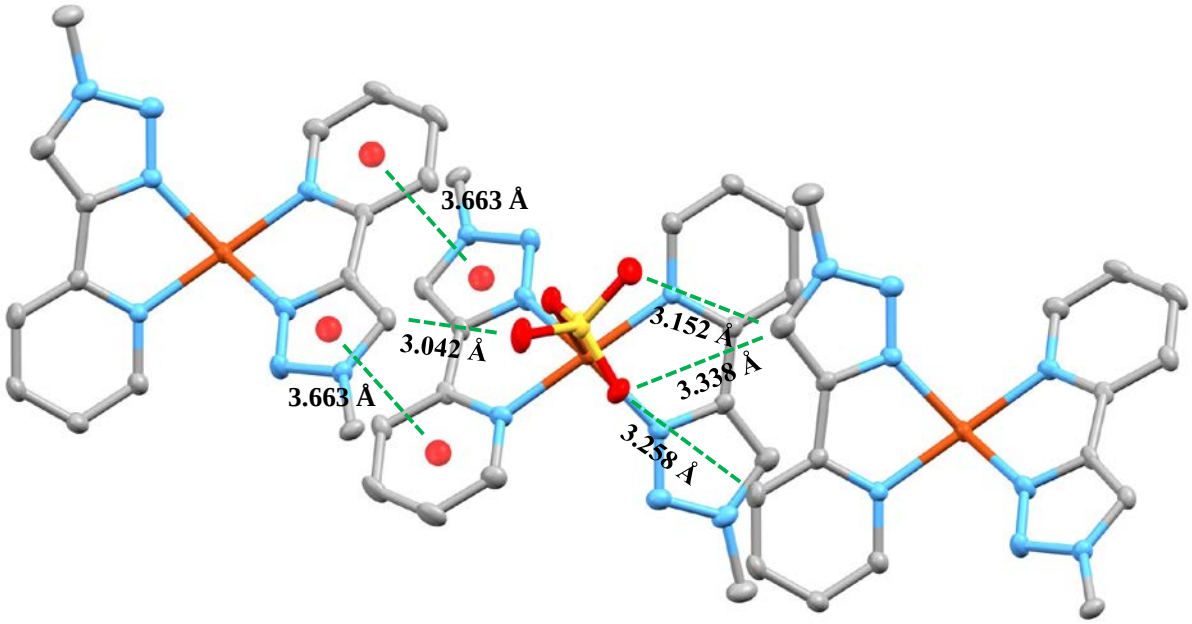

Fig. S21: Various intermolecular interactions present in [$\mathbf{L}_2Cu_2(SO_4)_2$].

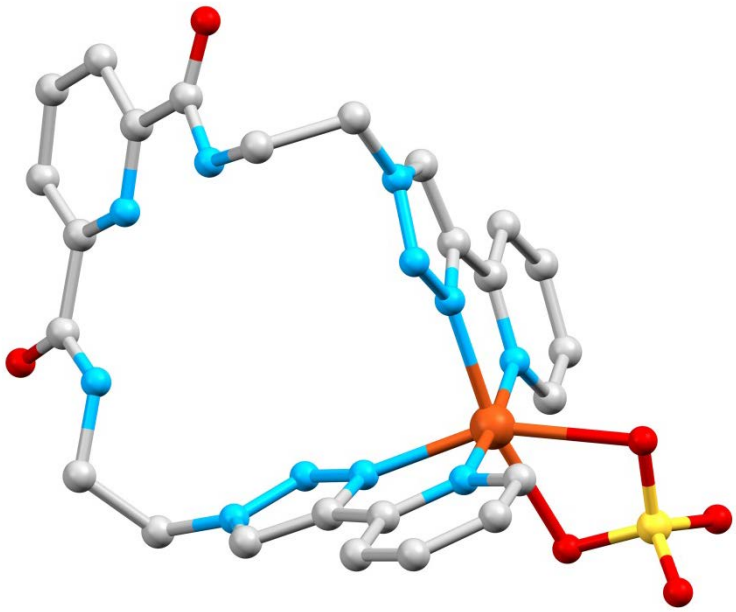

Fig. S22: Mononuclear Cu(II)-macrocycle of [$\mathbf{L}Cu(SO_4)$] (solvent molecules are removed for clarity).

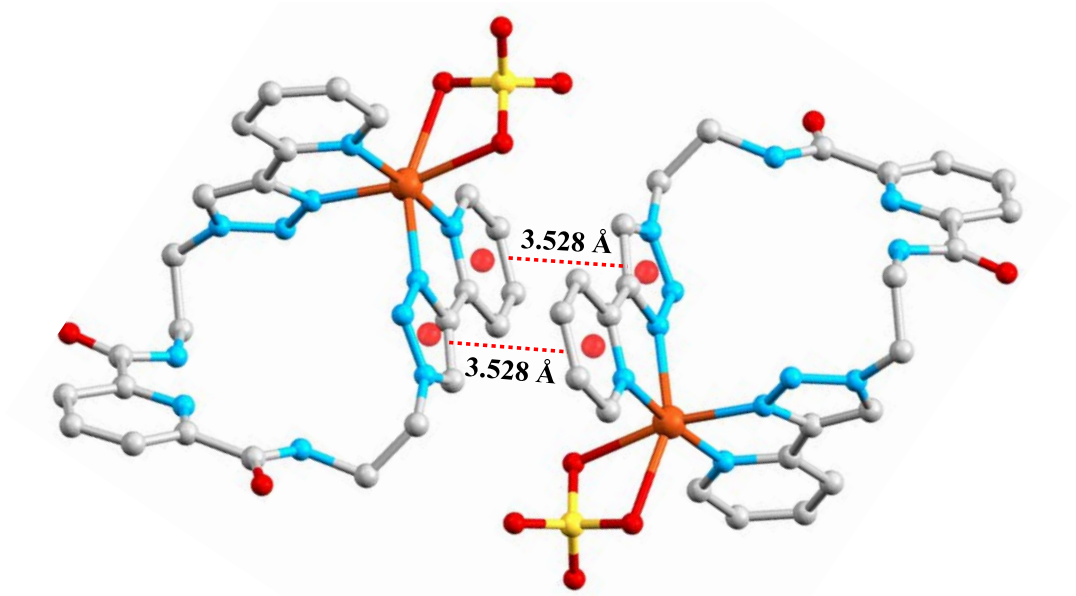

Fig. S23: Strong intermolecular π-π stacking interaction between two discrete units of mononuclear Cu(II)-macrocycle of [**L**Cu(SO_4)].

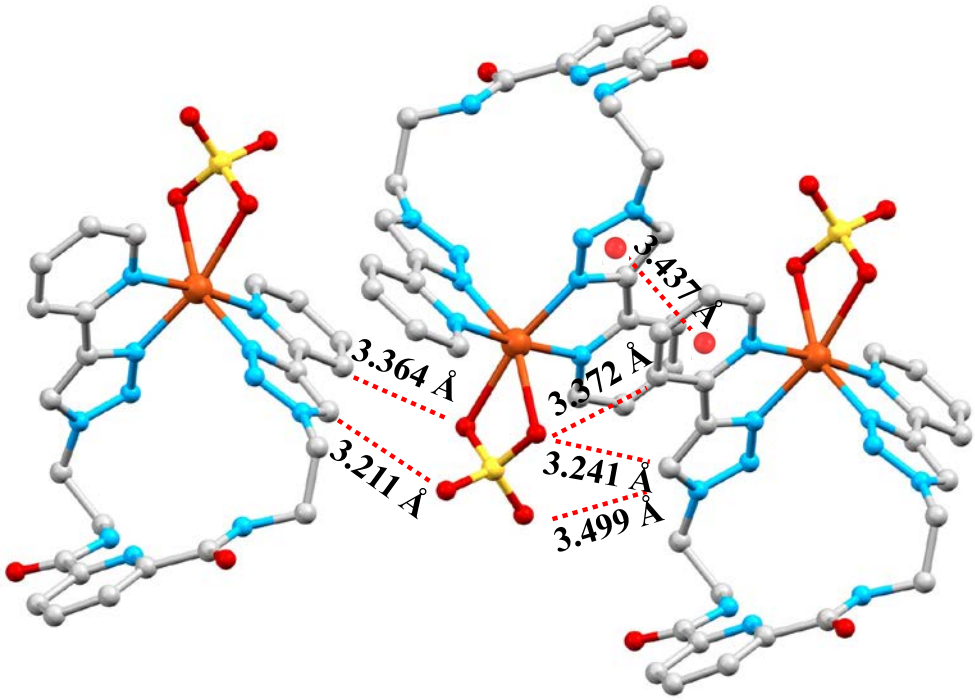

Fig. S24: Multiple intermolecular C-H···anion interaction is observed in the solid state packing in the crystal of [**L**Cu(SO_4)].

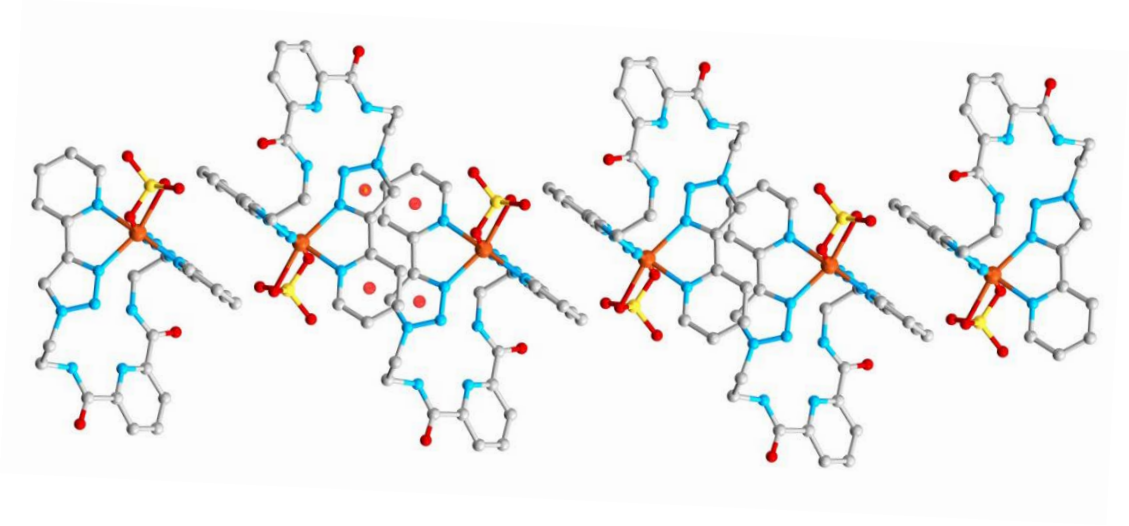

Fig. S25: Solid state supramolecular polymeric chain of macrocycle [**L**Cu(SO_4)].

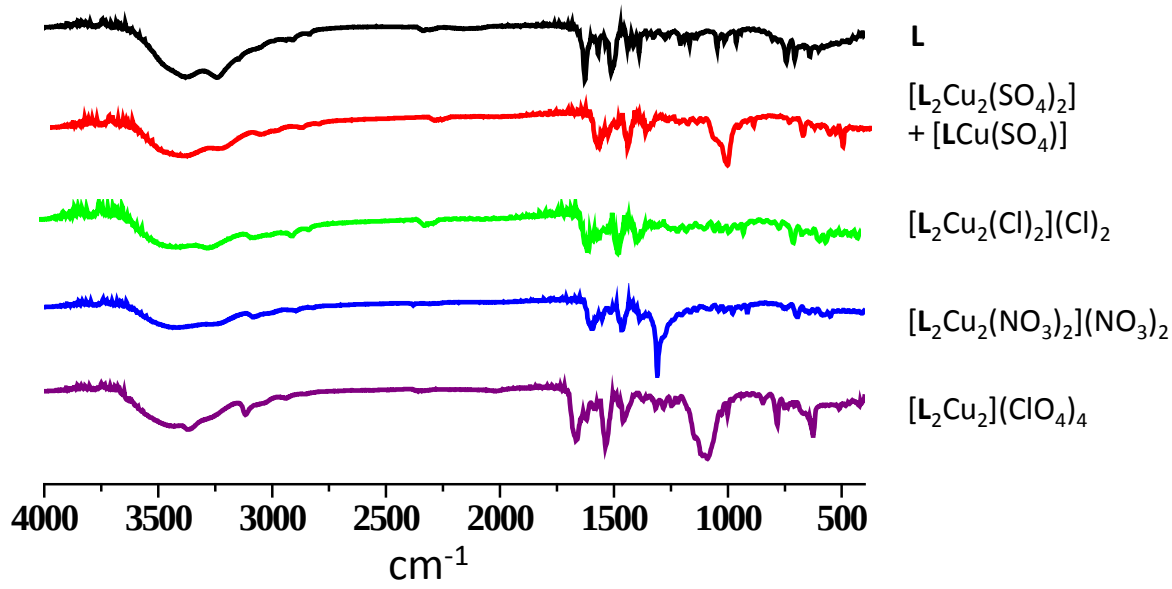

Fig. S26: IR spectroscopy study of free ligand and complexes.

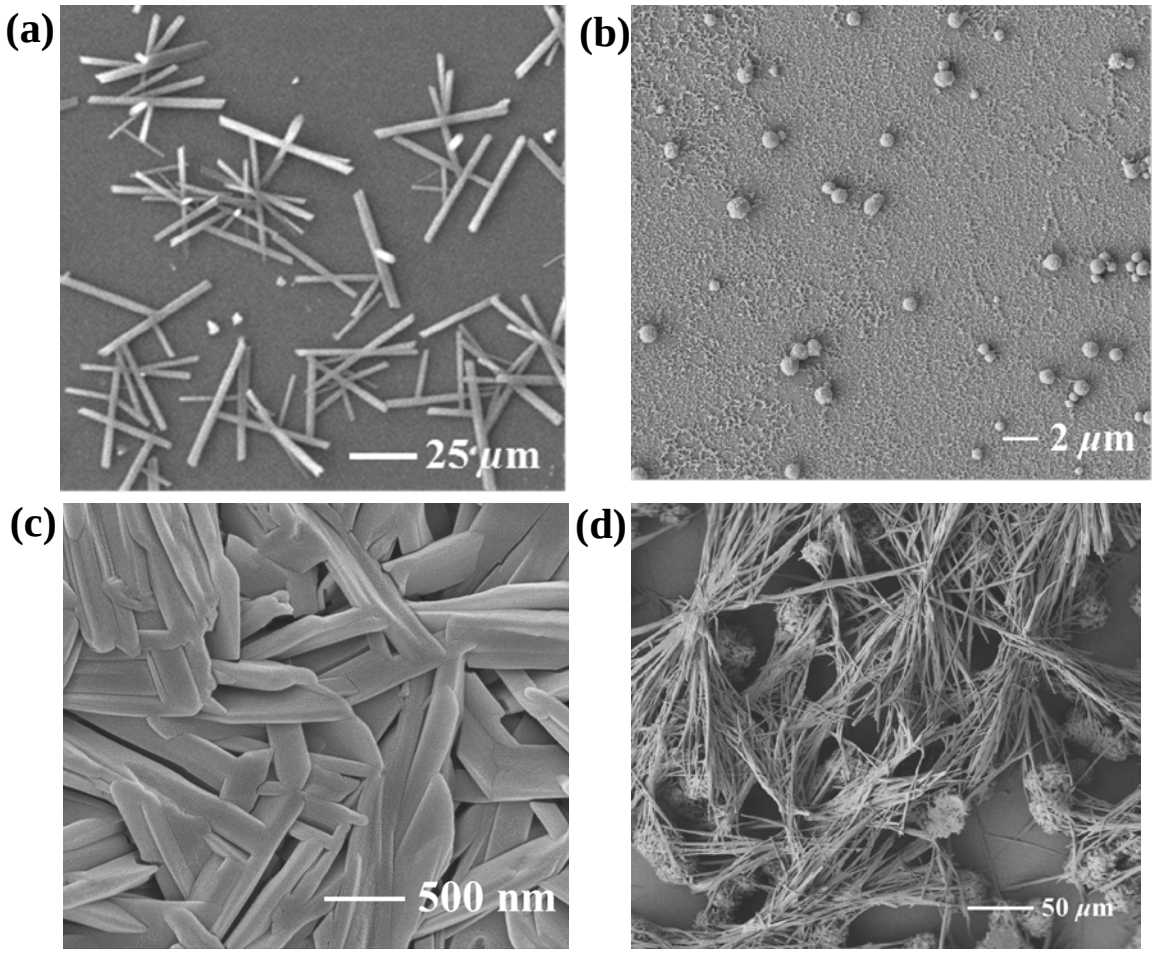

Fig. S27: (a) FESEM studies are performed with the solution prepared by addition of one equivalent of aqueous solution of different Cu(II)-salts like (a) $Cu(ClO_4)_2$, (b) $Cu(NO_3)_2$, (c) $CuCl_2$, (d) $CuSO_4$ with the DMF solution of **L** (~5 x 10^{-3} M) at 0.5:9.5 (v/v) at room temperature.

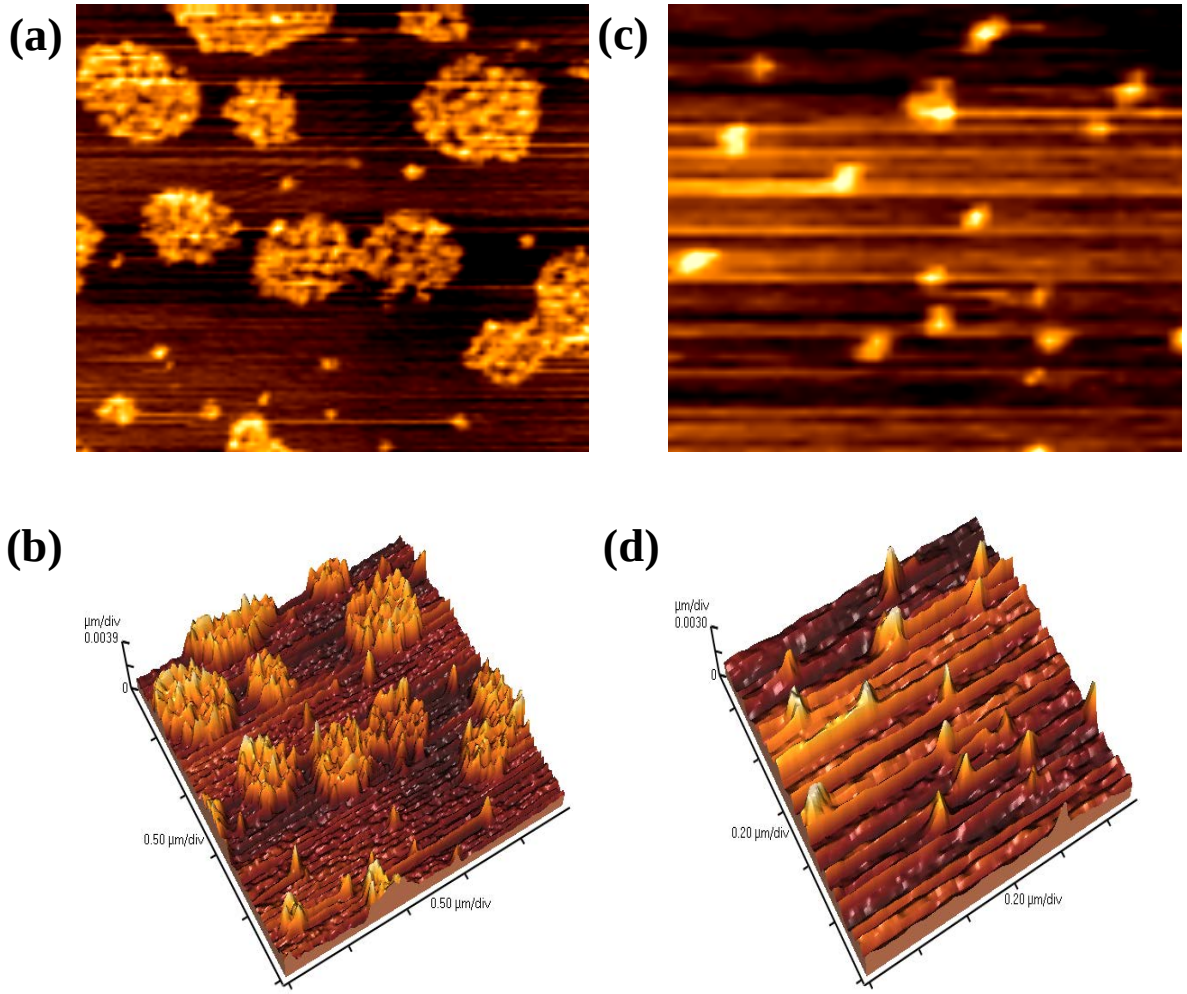

Fig. S28: (a,b) AFM study performed after the heating the DMF solution of $[\mathbf{L}_2Cu_2](ClO_4)_2$ at ~333 K, which shows micro-particle like assembly (2D and 3D view respectively) and (c,d) the micro-particle like assemble fully disassembled into nano-particles at ~353 K (2D and 3D view respectively).

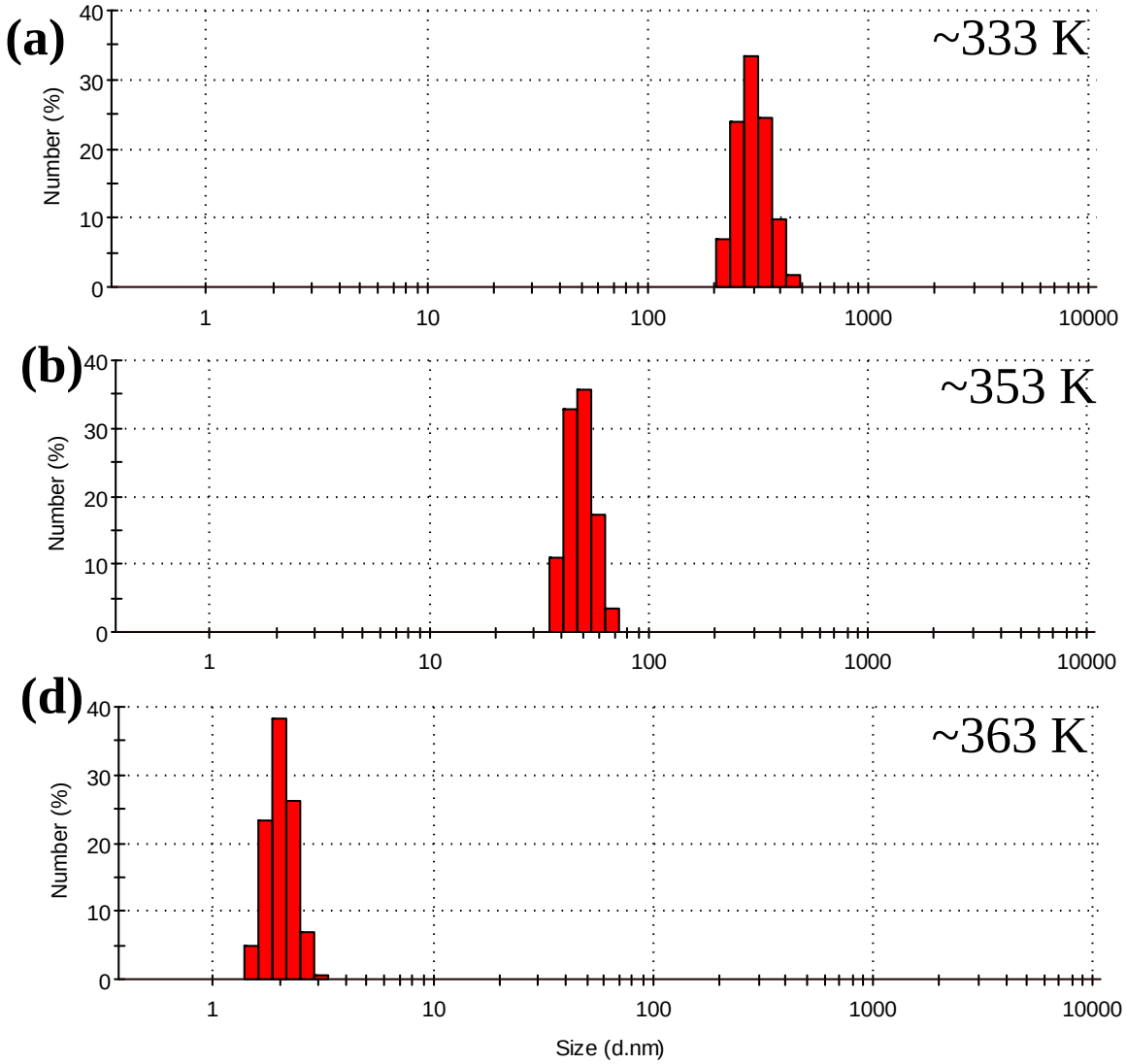

Fig. S29: Variable temperature dynamic light scattering study with the DMF solution of $[\mathbf{L}_2Cu_2](ClO_4)_2$, where the gradual decrease in particle-size is observed with temperature.

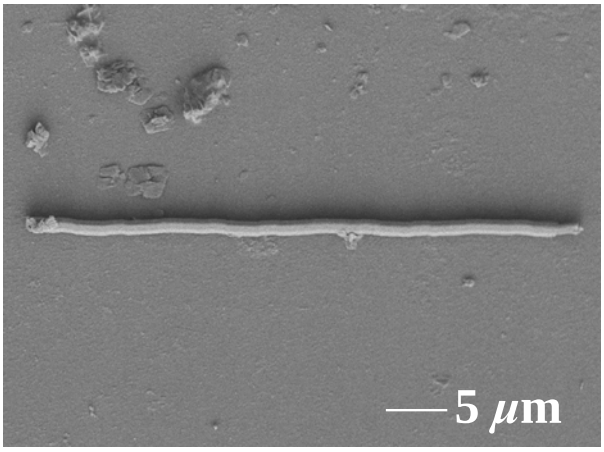

Fig. S30: The existence of rod-like assembly at ~313 K, though morphologically less pure than that of the room-temperature.

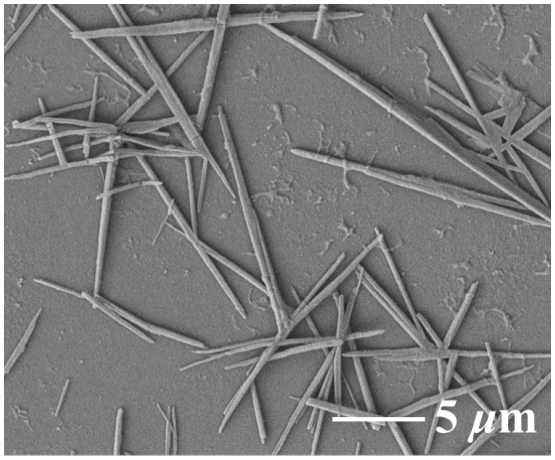

Fig. S31: Regeneration of rod-like assembly of $[\mathbf{L}_2Cu_2](ClO_4)_2$ from particle like assembly is observed in the FESEM study after 2 days of standing at room temperature.

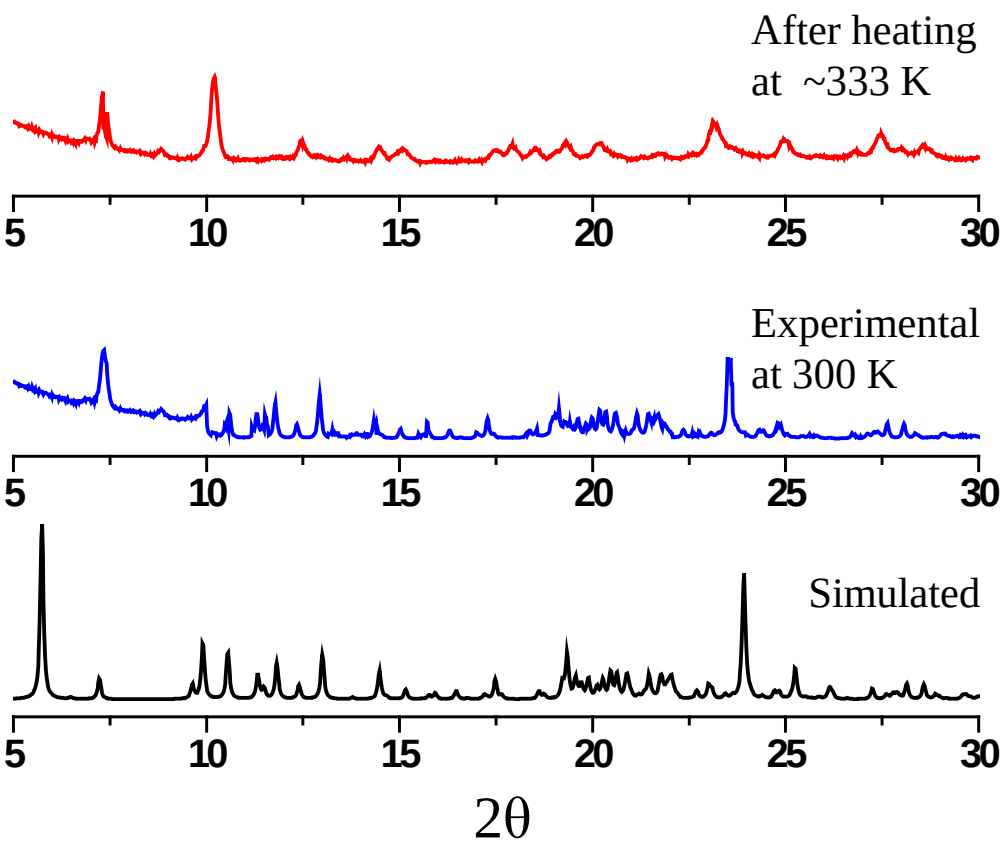

Fig. S32: PXRD study performed with the samples prepared from isolated single crystals shows the purity of **[**$\mathbf{L}_2Cu_2(ClO_4)_2$], further loss of different crystalline planes is also observed upon heating.

Table S1: Average M-N bond lengths (Å) at different coordination centres in different macrocyclic complexes.

Entry [a]	M-N(pyridine)		M-N(triazolyl)	
[$\mathbf{L}_3Cu_2$]$(ClO_4)_4$	Cu-N	2.016, 2.017	Cu-N	1.988, 1.988
[$\mathbf{L}_2Cu_2(NO_3)_2$]$(NO_3)_2$	Cu-N	2.035, 2.039	Cu-N	1.974, 1.989
[$\mathbf{L}_2Cu_2Cl_2$]Cl_2	Cu-N	2.016, 2.034	Cu-N	1.987, 2.003
[$\mathbf{L}_2Cu_2(SO_4)_2$]	Cu-N	1.978, 2.002	Cu-N	2.072, 1.991
[$\mathbf{L}$Cu(SO_4)]	Cu-N	2.026, 2.031	Cu-N	2.109, 2.128

Table S2: List of crystallographic parameter details of free ligand and complexes.

Compound reference	L	**[L**$_2$Cu$_2$(ClO$_4$)$_2$]	**[L**$_2$Cu$_2$(NO$_3$)$_2$](NO$_3$)$_2$	**[L**$_2$Cu$_2$(Cl)$_2$](Cl)$_2$	**[L**$_2$Cu$_2$(SO$_4$)$_2$]	**[L**Cu(SO$_4$)]
Chemical formula	$C_{25}H_{23}N_{11}O_3$	$C_{31}H_{37}Cl_2CuN_{13}O_{15}$	$C_{26}H_{23}CuN_{12}O_9$	$C_{52}H_{46}Cl_4Cu_2N_{20}O_4$	$C_{50}H_{46}Cu_2N_{22}O_{12}S_2$	$C_{28}H_{31}CuN_{12}O_7S$
Formula Mass	525.54	966.18	711.10	1283.97	1338.29	743.25
Crystal system	Orthorhombic'	Triclinic'	Triclinic'	Triclinic	Triclinic	Monoclinic'
a/Å	33.128(4)	9.5428(11)	10.317(3)	10.180(4)	10.431(3)	14.042(6)
b/Å	10.4228(11)	14.4035(16)	13.879(4)	13.691(4)	13.604(4)	25.506(12)
c/Å	18.122(2)	16.5243(18)	14.625(5)	13.928(4)	14.523(4)	10.718(5)
α/°	90.00	105.835(2)	110.491(7)	110.571(6)	113.317(7)	90.00
β/°	90.00	101.818(2)	109.527(7)	96.276(6)	97.646(8)	106.080(5)
γ/°	90.00	97.050(2)	99.837(8)	99.532(6)	97.790(8)	90.00
Unit cell volume/Å^3	6257.2(12)	2099.9(4)	1747.8(9)	1762.5(9)	1835.2(9)	3688(3)
Temperature /K	150(2)	150(2)	150(2)	150(2)	150(2)	150(2)
Space group	*Fdd*2	$P\bar{1}$	$P\bar{1}$	$P\bar{1}$	$P\bar{1}$	*P*2*(1)/c*
No. of formula units per unit cell, *Z*	8	2	2	1	1	4
Radiation type	MoKα	MoKα	MoKα	MoKα	MoKα	MoKα
No. of reflections measured	13831	19917	6674	19860	20429	29000
No. of independent reflections	2592	5338	6674	7638	5792	6663
R_{int}	0.0372	0.0485	0.0000	0.0565	0.0741	0.0904
Final R_1 values ($I > 2\sigma(I)$)	0.0972	0.0450	0.0656	0.0524	0.0486	0.0894
Final $wR(F^2)$ values ($I > 2\sigma(I)$)	0.2606	0.1318	0.1821	0.1392	0.1246	0.1966
Final R_1 values (all data)	0.1020	0.0625	0.1336	0.0782	0.0731	0.1346
Final $wR(F^2)$ values (all data)	0.2667	0.1443	0.2303	0.1556	0.1384	0.2126
CCDC number	1587666	1587667	1587668	1587669	1587670	1587671

References:

(1) SAINT; XPREP, 5.1 ed.; Sheldrick, G. M., Ed.; Siemens Industrial Automation Inc.: Madison, WI, 1995.
(2) SADABS, Empirical Absorption Correction Program; University of Göttingen: Göttingen, Germany, 1997.
(3) Sheldrick, G. M. SHELXTL Reference Manual: Version 5.1; Bruker AXS: Madison, WI, 1997.
(4) Sheldrick, G. M. SHELXL-97: Program for Crystal Structure Refinement; University of Göttingen: Göttingen, Germany, 1997.
(5) Spek, A. L. PLATON-97; University of Utrecht: Utrecht, the Netherlands, 1997.
(6) Mercury 3.7 (supplied with Cambridge Structural Database); CCDC: Cambridge, U.K., 2003−2004.
(7) Custelcean, R.; Bonnesen, P. V.; Duncan, N. C.; Zhang, X.; Watson, L. A.; Van Berkel, G.; Parson, W. B.; Hay, B. P. J. Am. Chem. Soc. **2012**, *134*, 8525.
(8) Puodziukynaite, E.; Oberst, J. L.; Dyer, A. L.; Reynolds, J. R. J. Am. Chem. Soc. **2012**, *134*, 968.